^{40}Ca photoneutron cross section above the giant dipole resonance

J. A. Eden*, G. J. O'Keefe, R. P. Rassool, D. J. McLean, and M. N. Thompson
School of Physics, The University of Melbourne, Parkville, Victoria 3052, Australia

T. Suda†, I. Nomura‡, J. Yokokawa, O. Konno, T. Terasawa, and Y. Torizuka
Laboratory of Nuclear Science, Tohoku University, Mikamine, Sendai 982, Japan
(Received 4 February 1991)

The ^{40}Ca(γ,n) reaction cross section has been measured with tagged photons with energies ranging from 31.2 to 102 MeV, for neutron emission angles of 45°, 60°, 75°, 90°, and 135°. Exclusive differential cross sections for the ^{40}Ca(γ,n) and ^{40}Ca(γ,p) reactions are found to be of a similar magnitude, but are not well predicted by recent random-phase-approximation and relativistic direct knock-out calculations. A quasideuteron model calculation with spin-orbit splitting of single-particle shells and an improved nucleon transparency correction is found to be consistent with the data. However, it is shown that this does not establish that the photoabsorption matrix element for the deuteron is necessarily similar to that of a correlated np-pair in nuclear matter. This result is generalized to question the predicted sensitivity to short-range correlations for photonuclear reactions calculated within the Gottfried factorization.

I. INTRODUCTION

To establish the relative importance of the various contributions to the transition amplitude for photonuclear reactions above the giant dipole resonance, it is necessary to assess the merits of many different theoretical models. The (γ,p) differential cross section has been predicted with reasonable accuracy using a variety of models [1–7] which embody quite different assumptions for the reaction mechanism. However, direct reaction models cannot predict cross sections for the (γ,pp), (γ,nn), or the dominant (γ,pn) reaction since the photon is assumed to couple to a single uncorrelated proton and cannot cause a one-body transition into a final state which has two nucleons in the continuum. In the simplest form of the shell model, the (γ,n) reaction requires the photon to interact with the neutron magnetization current. Because this interaction is much weaker than the interaction with the proton convection current, the (γ,n) cross sections are predicted to be much smaller than the (γ,p) cross sections. Experimentally, however, the (γ,n) and (γ,p) cross sections are of similar magnitude [8, 9] in light nuclei.

To make progress it is necessary to admit two-body effects into model calculations. This requires the inclusion of two-body terms in the nuclear current density (meson exchange terms) and the use of two-body wave functions constructed from properly correlated single-particle wave functons.

The first of these requirements is difficult to satisfy. In the static limit of a one-pion exchange potential ($\rho_{[2]}=0$), Siegert's hypothesis holds exactly, so that the continuity equation provides an implicit definition of all two-body terms in the nuclear current density and guarantees that the electromagnetic-interaction energy operator is gauge invariant. Hence the commutator $[\mathcal{H},\rho_{[1]}(\mathbf{r})]$ appearing in the leading term of the Siegert form of the electric transition operator will include meson exchange terms that are consistent with the choice of the NN-interaction embodied in the nuclear Hamiltonian. However, unless one adopts the long wavelength approximation, $qr \ll 1$, the second term in the transition operator is nonvanishing and requires an explicit description of the nuclear current density. Most microscopic calculations published to date adopt the long-wavelength approximation [5, 6] or truncate any explicit representation of the nuclear current density to include only the one-body terms [7].

Two-body wave functions that are constructed from a simple Clebsch-Gordan coupling of single-particle wave functions do not acknowledge the influence of the NN interaction. Short-range correlation functions can be introduced to suppress the amplitude of the two-body wave function at small NN separations, and thereby acknowledge the hard-core repulsion of the NN interaction. By assuming a direct reaction within the shell model, it has been argued [2, 10] that the ^{16}O(γ,p) and ^{16}O(γ,n) cross sections are accurately predicted when Jastrow [11] short-range correlation functions are included in the two-body wave functions. The predicted cross sections show extreme sensitivity to the free parameter appearing in the Jastrow function. A more recent calculation [12] of the ^{16}O(γ,pn) reaction cross section also finds considerable sensitivity to the parametrization of the Jastrow correlation function. However, in a more rigorous approach, correlation functions have been obtained by solving the Bethe-Goldstone equation, and are found to be of only minor consequence [13, 14] unless the reaction kinematics require the correlated nucleons to have very large bound-state momenta.

There is a clear need to obtain a comprehensive data set for specific reaction channels where shell-model calculations are expected to be reliable. A comparison of the (γ,n) and (γ,p) exclusive cross sections in lighter nuclei has been of critical importance in establishing the inade-

quacy of direct reaction models [3, 8, 9], but the existing data set is limited to only a few light nuclei. The aim of the present paper is to report the $^{40}Ca(\gamma, n)$ cross section for comparison with the existing $^{40}Ca(\gamma, p)$ cross section [15]. The $^{40}Ca(\gamma, n)$ data is compared with a number of microscopic theories, none of which adequately describes the data. Results from a quasideuteron model calculation appear to be consistent with the $^{40}Ca(\gamma, n)$ data, although it is argued that this says little about the basic photoabsorption matrix element. Extending this conclusion to the more general Gottfried factorization [16], the predicted sensitivity [12] to variations in the Jastrow correlation function is questioned.

II. EXPERIMENT

A. Experimental arrangement

The $^{40}Ca(\gamma, n)$ cross section reported in this paper was measured using the Tagged Photon Facility [17, 18] at the Laboratory for Nuclear Science, Tohoku University, Japan. The experimental arrangement is shown in Fig. 1. The facility provides tagged photons with energies ranging from 25.2 to 102 MeV, with an acceptance bin width of 2.6 MeV. A natural calcium (96.941% ^{40}Ca) target consisting of compressed turnings was located about 3 m downstream from the bremsstrahlung radiator. The cylindrical target, of diameter 72 mm, length 145 mm, and mass 735 g, was enclosed in a sealed plastic bag filled with argon gas. Individual neutron detector modules were located at angles of 45°, 60°, 75°, and 90° relative to the incident photon beam, and an assemblage of four neutron-detector modules was located at 135°. The neutron detector modules each subtended a solid angle of about 3.5 msr for detector-source separations of about 2.7 m, and were surrounded by plastic-scintillator (NE104) veto detectors.

B. Detectors

The neutron-detector modules used in the present experiment [9, 19] consist of a square block of aluminium, in which a cylindrical cavity has been bored and filled with an organic liquid scintillator (NE213). The cavity has a diameter of 180 mm and a depth of 103 mm. A Hamamatsu (R1250) photomultiplier tube is optically coupled to the glass window which seals the cavity. Rejection of all signals due to charged particles impinging on the neutron detectors was achieved by requiring an anticoincidence with signals from the immediately surrounding veto detectors. The remaining particle identification was therefore restricted to $n\backslash\gamma$ discrimination, which was achieved using two independent methods: first, by comparing the integrated charge of the neutron detector output for ADC gate widths of 20 and 200 ns, and second, by the standard pulse-shape discrimination (PSD) procedure using Canberra 2149A PSD modules. The PSD result is shown in Fig. 2, and was found to give clearer $n\backslash\gamma$ separation for the (more common) small pulse-height signals.

Neutron kinetic energies were determined by the time of flight (TOF) between the calcium target and the neutron detectors. The neutron kinetic energy resolution is obtained from the quadrature sum of the photon energy resolution, ± 1.8 MeV [19], and the neutron-TOF resolution, ± 1.4 ns, and results in uncertainties of ± 1.81 MeV at 9.32 MeV, ± 3.10 MeV at 48.7 MeV and ± 6.03 MeV at 84.0 MeV.

The dimensions of the veto detectors were selected to enclose the neutron detectors, but all have a common thickness of 2.0 cm. An assemblage of two veto detectors placed either side of a 1 mm sheet of lead was located in front of the 45° neutron detector in order to reduce the large number of events triggered by scattered bremsstrahlung photons interacting in the neutron detector. Consequently, it was necessary to make a small cor-

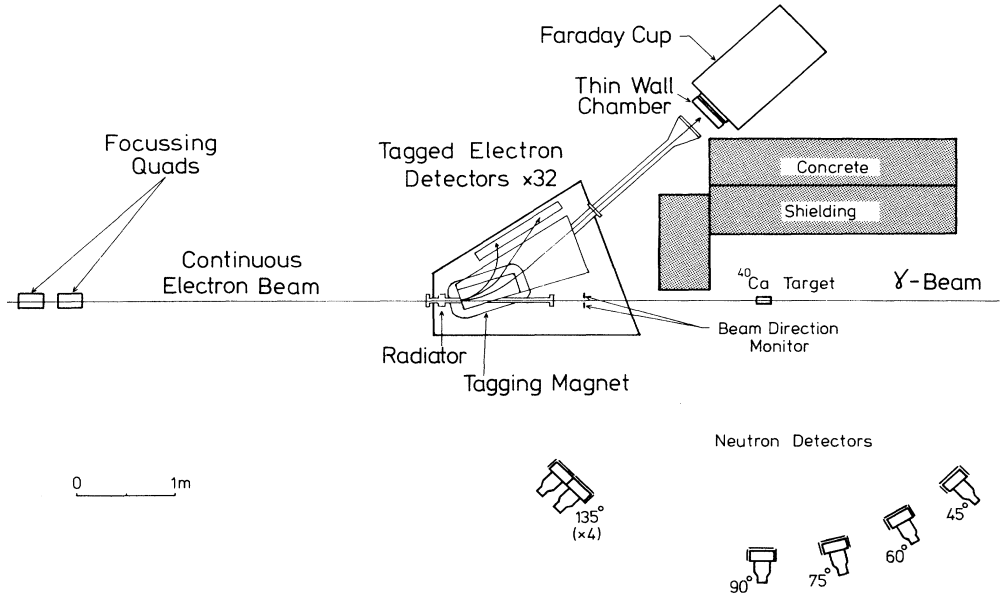

FIG. 1. Experimental arrangement for the $^{40}Ca(\gamma, n)$ cross-section measurement.

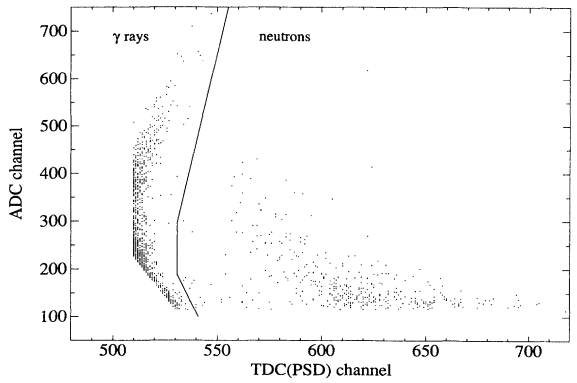

FIG. 2. Particle identification from pulse-shape discrimination. The distinct edge in the γ-ray distribution results from a preliminary cut in the off-line analysis.

rection for the loss of neutron flux reaching the neutron detector, but manageable data-acquisition rates were obtained without increasing the neutron-detector threshold from 3.15 MeVee (i.e., the pulse height corresponding to that produced by a 3.15 MeV electron).

C. Electronics and data acquisition

In the present measurement, data were recorded "event by event" with most electronic requirements being satisfied by standard fast NIM and CAMAC instrumentation. The event trigger required a neutron detector signal in anticoincidence with signals from any of the surrounding veto detectors, and in coincidence with a signal from any of the electron detectors in the tagging spectrometer. The photon energy responsible for the event was determined by identifying the electron channel that contributed to the event trigger. The neutron energy was calculated from the time interval between the neutron detector and tagged electron detector signals. For each event, ADC and PSD information was recorded for particle identification purposes. The data acquisition frequency was limited by the OKI 50/60 on-line computer, for which the maximum event rate was about 10 events per second for event sizes of about 24 bytes.

D. Collimation of the photon beam

Earlier tagged photon measurements at the Tohoku laboratory have been restricted to neutron emission angles of less than 90°. The inclusion of the neutron detectors at 135° required the removal of some of the concrete shielding. To investigate any consequent changes in the background contribution to the data, the target was removed and the TOF spectra were examined. A "γ-flash" peak was observed, resulting from the detection of photons scattered from the collimator. Although this photon background could be rejected by particle identification in the off-line analysis, any associated neutron background resulting from (γ, n) reactions in the collimator would contribute an unacceptable background to the TOF spectra. The problem was remedied by removing the collimator, and further background measurements confirmed that no "γ-flash" peak was observed in the TOF spectra measured at any angle.

The measurement of tagging efficiency (i.e., the fraction of the tagged photon flux which is incident on the target) requires the removal of the target and installation of a thick lead-glass Cherenkov photon detector. To obtain the tagging efficiency it is necessary to ensure that the photon beam is smaller than both the target and Cherenkov-detector dimensions. In previous experiments this was guaranteed since the photon beam was suitably collimated. However, in the present experiment the collimator was not used, so the measured efficiency as obtained from the Cherenkov detector does not give the true tagging efficiency.

A correction [20] to the measured tagging efficiency has been calculated using the theoretical expression for the bremsstrahlung angular distribution [21]. The position of the photon beam relative to the target axis was monitored by comparing the discriminated counts from thin plastic-scintillator detectors placed about the target, as shown in Fig. 1. The ratio of the discriminated counts was calibrated against the position of the incident electron beam on the bremsstrahlung radiator, and against the measured tagging efficiency, allowing a correction of order 10% which contributes an uncertainty of ~1% to the absolute scale of the double-differential cross section. A significant advantage in removing the collimator is that the true tagging efficiency is improved from a maximum value of ~50% to ~81% for all but the lowest photon energies; the average tagging efficiency under these conditions was 75%.

III. DATA REDUCTION

A. The absolute scale cross section

The double-differential cross section for the inclusive ^{40}Ca(γ, n) reaction is given by

$$\frac{d^2\sigma}{d\Omega_n dT_n}(E_\gamma, \theta_n, T_n) = \frac{N_n}{N_\gamma\, N_{\mathrm{Ca}}\, \xi\, \eta\, d\Omega\, dE_m}, \qquad (1)$$

where $N_n(E_\gamma, \theta_n, T_n)$ is the absolute number of photoneutrons with kinetic energy T_n emitted at an angle θ_n relative to the photon beam, which are detected in coincidence with a tagged photon of energy E_γ. The true/accidental coincidence ratio for N_n was in the range 5–8 for all detectors. The number of tagged photons $N_\gamma(E_\gamma)$ is given by the product of the number of tagged electrons and the corrected tagging efficiency, and has an uncertainty of 1%. The effective number of ^{40}Ca nuclei seen by photons at each tagged photon energy is given by $N_{\mathrm{Ca}}(E_\gamma)$ and carries an uncertainty of 2.6% resulting mainly from the uncertainties in the photon attenuation cross section and the target dimensions. The neutron-detector efficiency $\xi(T_n)$ was calculated using the program TOTEFF [22], and carries an uncertainty [19] of 7%. The solid angle and missing-energy bin sizes are given by $d\Omega(\theta_n)$ and dE_m, respectively.

B. Neutron transmission efficiencies

The neutron transmission efficiency η, giving the probability that a photoneutron produced in the target will not be scattered out of the solid angle subtended by a neutron detector, is given by the product of efficiencies for transmission through the target, the air separating the target and neutron detector, and the veto detector located in front of the neutron detector. For the 45°-neutron detector, an additional correction is required for the 1-mm lead sheet and second veto detector.

The neutron transmission efficiencies for the target, air, and lead sheet each take the form

$$\eta(\theta_n, T_n) = \exp[-\rho\sigma(T_n)t(\theta_n)], \tag{2}$$

where ρ is the density, σ is the neutron reaction cross section[23,24], and t is the thickness. For the calcium target, t is the mean transit distance for photoneutrons escaping the target at an angle θ_n, and assumes a distribution of photoneutron production sites in the target that is calculated from the photon attenuation cross section [25] and the bremsstrahlung angular distribution [21]. Typical values for the neutron transmission efficiencies in the calcium target, air, and 1 mm lead sheet are 0.93±0.6 %, 0.99±0.1 %, and 0.98±2 %, respectively.

If a neutron with a kinetic energy that is above the neutron-detector threshold (3.15 MeVee) suffers an interaction in a veto detector and the energy deposit in the veto detector gives a scintillation below threshold (1.06 MeVee), it is assumed that the neutron will retain sufficient energy to penetrate the veto detector, and that its angle of deflection is small enough to ensure that it subsequently hits the neutron detector, so that no correction is required. The transmission efficiency for the veto detectors is therefore taken as

$$\eta_{\text{veto}}(\theta_n, T_n) = 1 - \xi(\theta_n, T_n), \tag{3}$$

where ξ is the neutron detection efficiency for the veto detectors, as calculated with the program TOTEFF. The neutron-transmission efficiency for the veto detectors is typically about 0.96±7 %.

It is not possible to correct for the loss (or gain) of neutron flux at each angle due to elastic-scattering in the target because the ^{40}Ca(n,n) elastic scattering differential cross section is not well known at the neutron kinetic energies of interest. However, from the magnitude of the total elastic-scattering cross section [24] for ^{40}Ca , the total number of neutrons that suffer elastic-scattering collisions in the target can be estimated to be between 5 and 10%. This figure overestimates the required correction at any given neutron emission angle θ_n, since some of the elastically scattered neutrons will remain within the neutron-detector solid angle $d\Omega(\theta_n)$, and, more importantly, neutrons emitted at all other angles may be elastically scattered into the neutron detector solid angle. In the present analysis, no correction has been made for neutron elastic scattering. This is estimated to contribute a 5% uncertainty to the absolute scale of the double-differential cross section.

C. Correlations in the systematic uncertainties

The uncertainties in the neutron detector efficiency $\delta\xi/\xi$, and in the neutron transmission efficiency through the veto detectors $\delta\eta_{\text{veto}}/\eta_{\text{veto}}$, are anticorrelated, since an underestimation of ξ would ensure an overestimation of η_{veto}. Hence the two major sources of uncertainty in the absolute scale of the double-differential cross section tend to cancel, leaving an uncertainty of only 6.7% in the product $\xi\eta_{\text{veto}}$. The fractional systematic uncertainty in the cross section is taken as the quadrature sum of the fractional uncertainties in $\xi\eta_{\text{veto}}$, η_{Ca}, η_{air}, N_{Ca}, N_γ, and the 5% uncertainty resulting from the neglect of neutron elastic scattering. The total systematic uncertainty for the ^{40}Ca(γ,n) cross-section measurement is 9%.

IV. RESULTS AND DISCUSSION

A. Double-differential cross sections

1. *Missing energy spectra*

Missing energy for the ^{40}Ca(γ,n) reaction is defined as

$$E_m = E_\gamma - T_n - T_R - Q, \tag{4}$$

where E_γ is the photon energy, T_n and T_R are the kinetic energies of the neutron and recoiling ^{39}Ca nucleus, respectively, and Q is the ^{40}Ca$(\gamma,n)^{39}$Ca reaction threshold. The ^{40}Ca(γ,n) missing-energy spectra (i.e., the cross sections, differential in missing energy and neutron-emission angle) are presented in Fig. 3 for laboratory-frame neutron-emission angles θ_n = 45°, 60°, 75°, 90°, and 135°. To obtain statistically significant results, it was necessary to average the missing-energy spectra from several different tagged photon energies, as is indicated in the figure.

In the *exclusive* region of the missing-energy spectra, $E_m < 5.8$ MeV, only the ^{40}Ca$(\gamma,n)^{39}$Ca reaction contributes to the data. In the *inclusive* region, $E_m >$ 5.8 MeV, a variety of reaction channels may contribute, for example, the ^{40}Ca$(\gamma,pn)^{38}$K, ^{40}Ca$(\gamma,nn)^{38}$Ca, and ^{40}Ca$(\gamma,dn)^{37}$K reaction channels open at E_m=5.8, 13.4, and 15.6 MeV, respectively.

At the lower photon energies (E_γ=31.2 to 57.9 MeV) the data are dominated by electric-dipole transitions to collective states. The resolution of the averaged missing energy spectra does not permit identification of the discrete final states.

At higher photon energies (E_γ=60.5 to 102 MeV) the exclusive ^{40}Ca(γ,n) cross section becomes extremely small. In the inclusive region, the data are largely the result of (γ,pn) reactions, and the shape of the missing-energy spectra is determined by the available phase space. In view of the dominance of the (γ,pn) reaction, the data are compared with the results of a quasideuteron model (QDM) calculation, as discussed below.

2. *Comparison with quasideuteron model calculation*

The QDM double-differential cross section for the inclusive (γ,n) reaction leading to the emission of an np pair from the orbitals $(nlj;n'l'j')$ is given by [20]

$$\left.\frac{d^2\sigma_{qdm}}{dT_n d\Omega_n}\right|_{nlj;n'l'j'} = c' L \frac{N_{nlj} Z_{n'l'j'}}{A} \int F_{nln'l'}(p_q) \left\{ \frac{d\sigma_d(E'_\gamma, \vartheta''_n)}{d\Omega''_n} \right\} \delta_{T_n} J_n \, d\mathrm{p}_q, \tag{5}$$

where N_{nlj} is the number of neutrons in the (nlj) orbital, $Z_{n'l'j'}$ is the number of protons in the $(n'l'j')$ orbital, A is the number of nucleons in the target nucleus, $F_{nln'l'}(p_q)$ is the unit-normalized momentum density for a quasideuteron formed from a neutron in the (nlj) orbital and a proton in the $(n'l'j')$ orbital, $\{d\sigma_d/d\Omega''_n\}$ is the deuteron differential cross section, evaluated in the center-of-momentum (c.m.) frame of the (internal) neu-

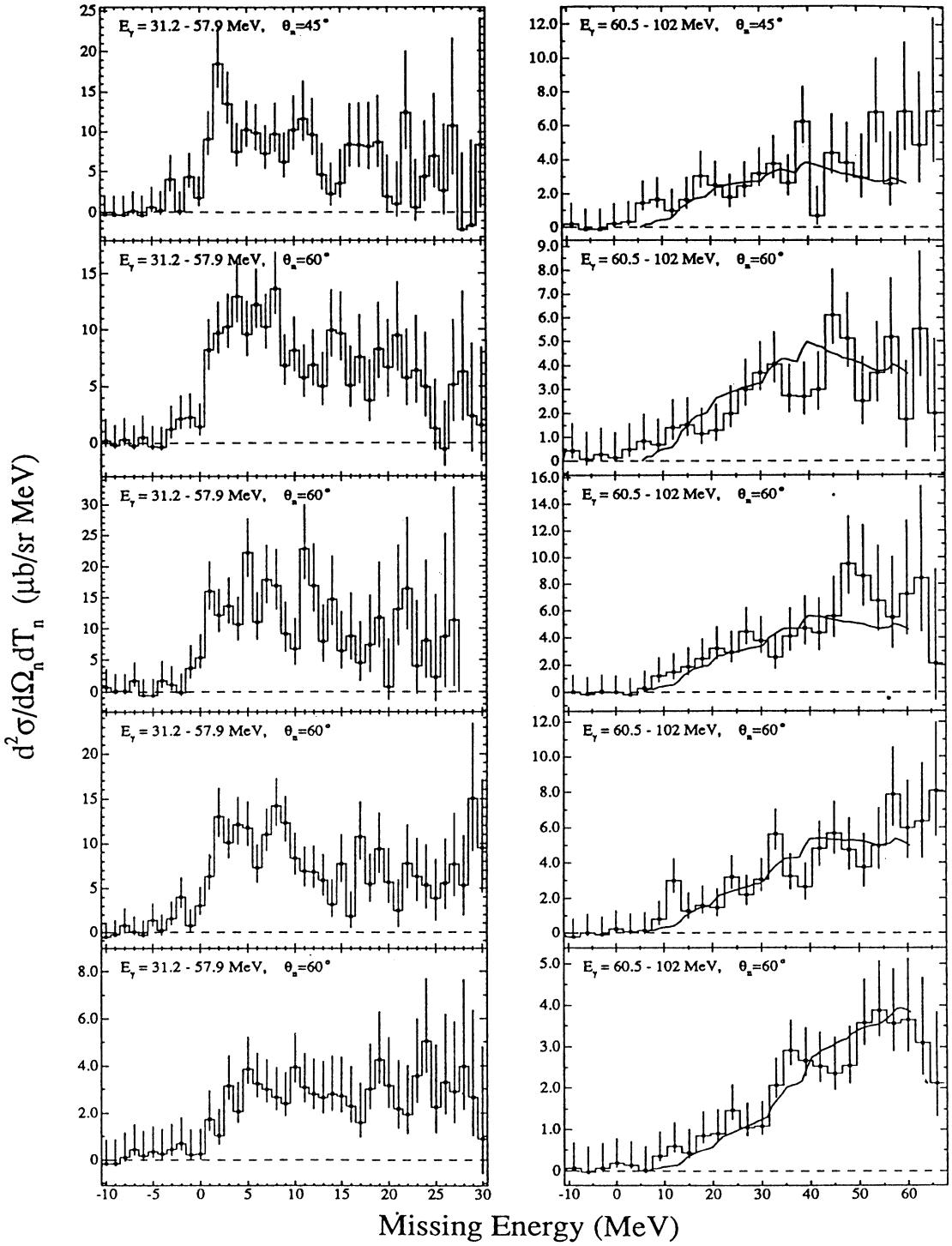

FIG. 3. ^{40}Ca(γ, n) missing-energy spectra. The solid curve is the result of a QDM calculation at $E_\gamma = 80$ MeV.

tron and proton, E'_γ is the photon energy, Doppler shifted into the frame where the quasideuteron is at rest, ϑ''_p is the angle between the photon and (internal) proton momenta, calculated in the c.m. frame, J_n is the product of Jacobians required for the coordinate transformations, L is the Levinger parameter, and c' is a normalization constant, chosen so that

$$\sigma_{\rm QDM} = L\,\frac{NZ}{A}\,\sigma_d. \tag{6}$$

The present calculation acknowledges spin-orbit splitting for the neutron and proton single particle energies. The double-differential cross section for the inclusive (γ, n) reaction in an A-particle nucleus is,

$$\frac{d^2\sigma_{\rm QDM}}{dT_n d\Omega_n} = \sum_{nlj;n'l'j'} \eta_{nl}(T_n) \left\{ \frac{d^2\sigma_{\rm QDM}}{dT_n d\Omega_n}\bigg|_{nlj;n'l'j'} \right\}. \tag{7}$$

The sum over bound-state orbitals in Eq. (7) is modified by the neutron transparency η_{nl}, which is usually taken as a constant [3, 9]. In the present calculation, however, the neutron transparency depends on the neutron kinetic energy, and, more importantly, the orbital from which the neutron is ejected, and is given[20] by a simple development of earlier treatments [26, 27] as

$$\eta_{nl}(Tn) = \frac{\int \rho_{nl}(r)\exp\left(-\sigma_{nn'}(T_n)\int_{t=0}^{\infty}\rho_A(r'(t))dt\right)d\mathbf{r}}{\int \rho_{nl}(r)d\mathbf{r}}. \tag{8}$$

The neutron transparency is shown in Fig. 4. The volume integrations in Eq. (8) extend over all space. The photoneutron escape trajectory is defined to start at the photoabsorption site (r, θ, ϕ), and be directed towards the detector. The nuclear density at position t on the escape trajectory is denoted with $\rho_A(r'(t))$, and $\rho_{nl}(r)$ is the density of nucleons in the harmonic-oscillator shell (nl) at radius r. The cross section $\sigma_{nn'}(T_n)$, for a neutron of kinetic energy T_n, interacting with the residual $(A-2)$ nucleus is approximated by the ^{40}Ca neutron reaction cross section [24]. The neutron transparency of Eq. (8) can be generalized to other particles by an appropriate choice of $\sigma_{nn'}$.

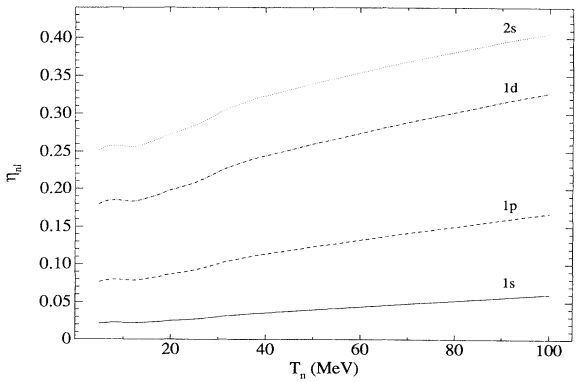

FIG. 4. Neutron transparency for specified harmonic-oscillator shells.

Figure 3 shows that the QDM results appear to account for a very large fraction of the cross section in the inclusive region of the missing energy spectra. In a similar fashion to earler QDM calculations [3], the absolute scale of the QDM is set by normalizing to the missing energy data at θ_n=135°, where the cross section for the (γ, pn) reaction is expected to be much larger than that of the (γ, n). The predicted strength and shape at all angles appears to be in good agreement with the data. The well-established success of the QDM in predicting the inclusive (γ, n) spectra in light nuclei [3, 8, 9] is now extended to mass A=40.

B. Exclusive differential cross sections

1. *Comparison of $^{40}Ca(\gamma, n)$ and $^{40}Ca(\gamma, p)$ data*

A comparison of the relative magnitudes of the exclusive (γ, n) and (γ, p) reactions has long been recognized as an important test of the photoreaction mechanism [3]. Since the exclusive ^{40}Ca$(\gamma, p)^{39}$K differential cross section has already been measured [15] for the excitation energy intervals E_X=0.0, 2.5–3.5, and 3.5–8.0 MeV, this comparison is now possible for ^{40}Ca. The exclusive ^{40}Ca(γ, n) differential cross sections were obtained by integrating the missing-energy spectra from $E_m = -2.5$ to 3.5 MeV, and thus refer to the ^{40}Ca$(\gamma, n)^{39}$Ca reaction leading to population of the ground and first three excited states in ^{39}Ca. The results are given in Table 1, and compared with the ^{40}Ca(γ, p) differential cross section (for the excitation energy interval 0.0–3.5 MeV) in Fig. 5. The measured cross sections for the exclusive reactions ^{40}Ca(γ, n) and ^{40}Ca(γ, p) are essentially the same within the statistical precision.

2. *Comparison with random-phase-approximation (RPA) calculations*

Within an RPA framework, Ryckebusch *et al.* [7] have calculated differential cross sections for the reactions (γ, p_0), (γ, p_1), (γ, n_0), and (γ, n_1) in ^{40}Ca (and ^{16}O).

TABLE I. ^{40}Ca(γ, n) exclusive differential cross sections for the missing-energy region $E_m = -2.5$–3.5 MeV. The scale uncertainty is 9%.

$E_\gamma = 33.7 - 47.6$ MeV		$E_\gamma = 50.2 - 70.9$ MeV	
θ_n (deg)	$d\sigma/d\Omega$ (μb/sr)	θ_n (deg)	$d\sigma/d\Omega$ (μb/sr)
45	$59.2^{+8.5}_{-6.8}$	45	$13.1^{+4.8}_{-2.9}$
60	$44.8^{+6.5}_{-5.3}$	60	$9.1^{+3.8}_{-2.3}$
75	$71.2^{+10.4}_{-8.4}$	75	$7.6^{+4.7}_{-2.5}$
90	$44.4^{+6.1}_{-5.2}$	90	$4.3^{+3.2}_{-1.7}$
135	$4.6^{+1.8}_{-1.1}$	135	$0.54^{+1.55}_{-0.49}$

The results for the $^{40}Ca(\gamma, n_0)$ and $^{40}Ca(\gamma, p_0)$ reactions are shown in Fig. 5 and are seen to significantly overestimate the differential cross sections at forward angles. This excess strength is expected to arise from the simplistic single-particle description of the final-state wave function since a linear combination of particle-hole admixtures would not, in general, interfere coherently. The need for a large (up to 8-particle–8-hole) basis space has been emphasized in a previous shell-model calculation [28] which determined the energies of the $J^\pi = 0^+$ states in ^{40}Ca.

An earlier RPA calculation by Cavinato *et al.* [6] predicts smaller $^{40}Ca(\gamma, n_0)$ and $^{40}Ca(\gamma, p_0)$ cross sections, and appears to agree with the data. However, both of the RPA calculations shown in Fig. 5 refer to reactions leading exclusively to population of the ground states of ^{39}K and ^{39}Ca, whereas the data are the sum of the differential cross sections for population of the ground and first three excited states.

The RPA prediction of the relative magnitudes of the (γ, p_0) and (γ, n_0) cross sections appears to be consistent with the data, although the statistical uncertainty in the experimental results at large nucleon emission-angles limits the scope of this conclusion.

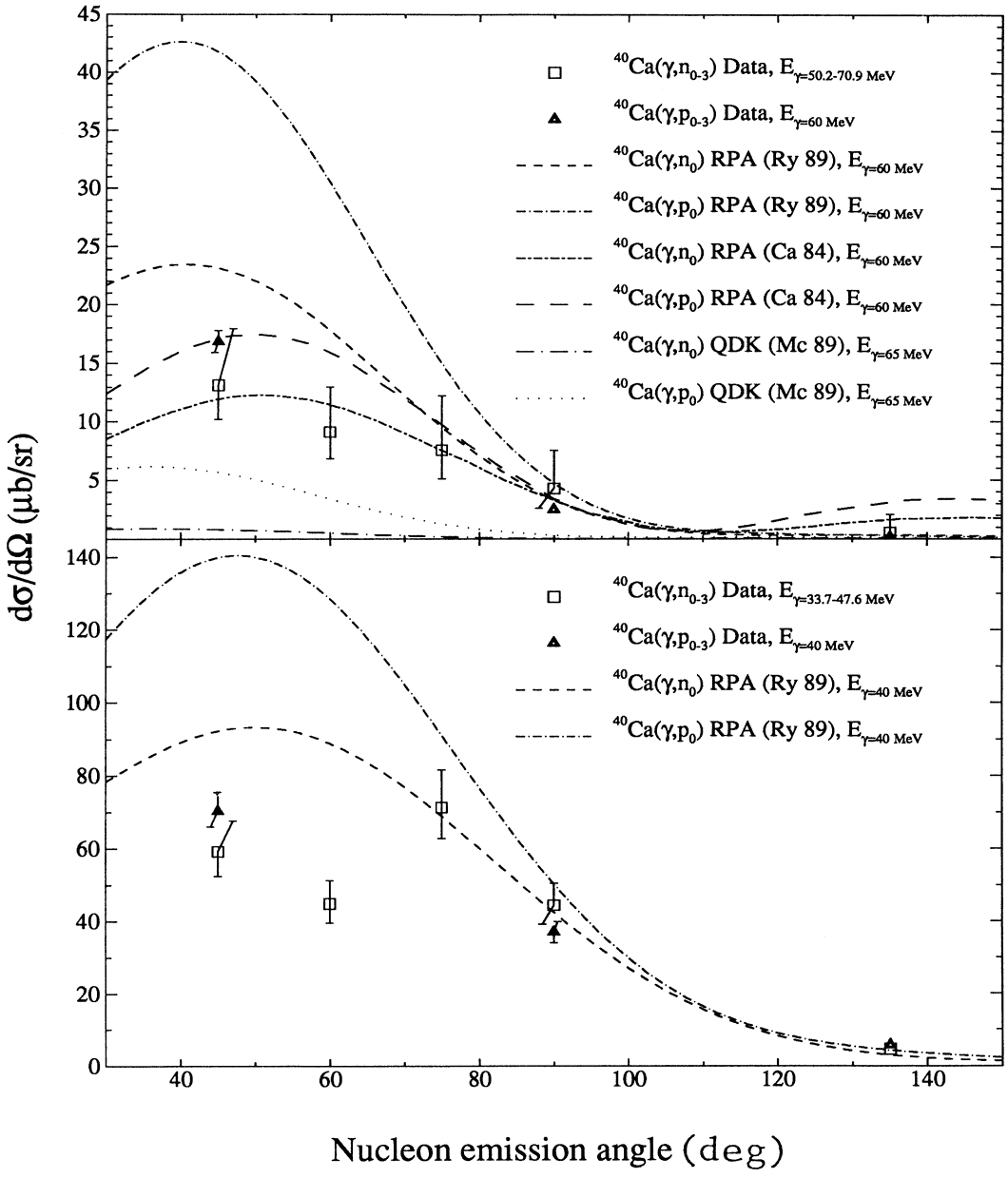

FIG. 5. $^{40}Ca(\gamma, n)$ and $^{40}Ca(\gamma, p)$ exclusive differential cross sections.

3. Differences in RPA calculations

It is surprising to find that two similar RPA calculations give such different results. Both are coordinate-space calculations using a Skyrme nucleon-nucleon interaction, and appear to be limited to a one-particle–one-hole description of the excited states in ^{40}Ca. Both calculations employ a multipole expansion of the electromagnetic field, and use very similar multipole-effective charges. However, the calculations do have some differences. Foremost among these is the description used for the electric transition operator, defined [29] for a photon with momentum $\mathbf{q}$ and polarization λ as

$$T_{\rm el}^{[L]}(q,\lambda) = \frac{i^L}{q}\int \nabla \times \{j_L(qr)\mathbf{Y}_{LL,\lambda}(\hat{r})\}\cdot\mathbf{j}(\mathbf{r})\,d\mathbf{r}. \quad (9)$$

The Siegert form of this is

$$T_{el}^{L}(q,\lambda) = -\frac{i^L}{q\sqrt{L(L+1)}}\int [\mathcal{H},\rho(\mathbf{r})]\left(1+r\frac{d}{dr}\right) j_L(qr)\mathbf{Y}_{LL,\lambda}(\hat{r})\,d\mathbf{r} + \frac{q\,i^{L+1}}{\sqrt{L(L+1)}}\int \mathbf{r}\, j_L(qr)\mathbf{Y}_{LL,\lambda}(\hat{r})\cdot\mathbf{j}(\mathbf{r})\,d\mathbf{r}. \quad (10)$$

Cavinato uses the long-wavelength approximation (LWA) so that the second term in Eq. (10) drops out with $qr \ll 1$, thereby eliminating the only explicit reference to the total nuclear current density $\mathbf{j}(\mathbf{r})$. Meson-exchange currents are implicitly included [30] by the commutator appearing in the first term of Eq. (10) since, within Siegert's hypothesis ($\rho_{[2]}$=0) the continuity equation becomes

$$\nabla\cdot(\mathbf{j}_{[1]}+\mathbf{j}_{[2]}) + i\,[\mathcal{H},\rho_{[1]}] = 0. \quad (11)$$

Equation (11) must hold for a gauge-invariant description of the electromagnetic interaction, and implies a nonvanishing $\mathbf{j}_{[2]}$ for any NN potential with isospin or momentum dependence i.e., whenever the two-body term in the commutator is nonzero.

For 80 MeV photons, where $qr \sim 1.5$, the LWA is not valid. Ryckebusch avoids the LWA by retaining the second term in Eq. (10), but truncates the full nuclear current density to include only the one-body part. This suggests that the meson-exchange contribution to both calculations should be about the same, but, in the approach taken by Ryckebusch, the one-body terms are less effected by the failing of the LWA. Ryckebusch concludes that the LWA may seriously underestimate the total photoabsorption cross section. Unfortunately both the Cavinato and the Ryckebusch calculations retain the use of multipole-effective charges (derived in the LWA) rather than explicitly acknowledging [31] that the residual nucleus and continuum nucleons have a total momentum $\mathbf{q}$ relative to the initial nuclear state.

4. Comparison with quasidirect knock-out calculation

McDermott [32] has calculated the cross sections for the (γ,n_0) and (γ,p_0) reactions using a relativistic quasidirect knock-out (QDK) approach. The results for ^{40}Ca are shown in Fig. 5.

Boffi [31] has investigated the importance of a number of approximations, which are commonly adopted in direct-reaction calculations, and has provided detailed prescriptions for future treatments. It is not clear whether McDermott's calculation includes the recoil term in the transition amplitude, or observes the requirements of a properly orthoganalized final-state wave function.

McDermott regards his calculation as "exploratory," and implies that the many deficiencies might be remedied in future publications. Even if this is so, it seems inevitable that future calculations will continue to depend sensitively on the choice of optical-model parameters used to approximate the final-state interaction. These parameters are not well known, and for one of the published parameter sets, McDermott finds that the relativistic results are worse than the nonrelativistic ones. It may be that the variation of the cross section with changes to the optical-model parameters is influenced by the alterations to the orthogonality defect of the final-state wave function.

The relativistic QDK model fails to predict the observed similarity in the magnitudes of the ^{40}Ca(γ,n) and ^{40}Ca(γ,p) cross sections; the ^{40}Ca(γ,n) cross section is underestimated by about an order of magnitude.

C. Inclusive differential cross sections

The double differential cross sections for the inclusive ^{40}Ca(γ,n) reaction, as presented in Fig. 3, are integrated over the missing energy interval 6–60 MeV to give the results presented in Table II and Fig. 6.

The QDM calculation of the differential cross section for the inclusive ^{40}Ca(γ,n) reaction is obtained by integrating Eq. (7) over all neutron energies, or, equivalently, by integrating over the missing-energy interval E_m=6–60 MeV. The scale of all QDM results presented in the present paper is set with L=11.4±1.1 and c'=1.48. These values are similar to those reported in an earlier QDM calculation [3], although as will be discussed in the following section, it is unlikely that this has any physical significance.

D. *NN* correlations

1. Physical significance of the QDM

The longstanding success of the QDM in predicting the cross sections for a number of different reaction channels over a wide range energies and nucleon emission angles [3,9,33–38] is usually interpreted as evidence that the deuteron and quasideuteron photoabsorption ma-

TABLE II. ^{40}Ca(γ, n) inclusive differential cross sections for $E_\gamma = 60.5 - 102$ MeV, and missing-energy interval $6 - 60$ MeV. The scale uncertainty is 9%.

θ_n (deg)	45	60	75	90	135
$d\sigma/d\Omega$ (μb/sr)	173 ± 12	152 ± 9	237 ± 16	195 ± 10	102 ± 4

trix elements are very similar. However, this interpretation seems questionable since it is not possible for all nucleon-nucleon correlations in nuclear matter to share the restricted spectroscopic description that is found in the deuteron (i.e, an antisymmetric wave function constructed by coupling two fermions of orbital angular momentum l and l' to a total orbital angular momentum, spin and isospin of L, S T, is nonvanishing only if $l+l'+L+S+T$ is an odd integer). The lack of spectroscopic correspondence between the deuteron and quasideuteron suggests that the photoabsorption probability for the pn pair is misjudged in the QDM, and that the success in predicting the opening angle distributions [33–35,38] for the (γ, pn) reaction results from the dominance of the momentum density [16] in the expression for the QDM cross section. To illustrate this quantitatively, the QDM has been used to predict the (γ, pn) angular correlation function, i.e., the cross section, differential in the emission angles and integrated over the energies of both photonucleons in the ^{40}Ca(γ, pn) reaction. The solid curve shown in Fig. 7 is the standard QDM result for a photon interacting with a quasideuteron formed from an np pair in the $1d_{3/2}$ orbital. The dashed curve differs from this only in that the differential cross section for the photodisintegration of the deuteron has been set to a constant. Since the absolute scale cannot be predicted by the QDM, and is irrelevant for the present considerations, the results have been normalized to have equal strength. The dominance of the momentum density can also be seen in a phase-space analysis of the QDM prediction of the ^{12}C(γ, pn) angular-correlation function [38].

The "success" of the QDM in predicting (γ, pn) angular-correlation data results mainly from the fact that the momentum density $F(p_q)$ gives a reasonable estimate of the momentum distribution of the bound-state np-pair, and does not require the quasideuteron and deuteron photoabsorption matrix elements to be similar. Even quite serious errors in the estimation of the photoabsorption probability are unlikely to be revealed by comparing the QDM results with (γ, pn) angular-correlation data, and can be partially hidden by an appropriate choice for the Levinger parameter.

2. *The Gottfried factorization*

The insensitivity of the QDM cross section to the photoabsorption probability can be generalized to any Gottfried factorized [16] (γ, pn) cross section,

$$d\sigma = (2\pi)^{-4} F(p_q) S_{fi} \delta(E_f - E_i) d\mathbf{p}_n d\mathbf{p}_p. \quad (12)$$

The QDM expression for the (γ, pn) cross section is a special case of Eq. (12), obtained by replacing S_{fi} with the deuteron cross section, transformed into the appropriate frame. Hence the conclusions of the previous section can be generalized: Figure 7 shows that S_{fi} varies slowly compared to $F(p_q)$ in any Gottfried-factorized (γ, pn) cross section.

Short-range correlations have generally [2, 10] been treated by introducing a Jastrow function [11] to suppresses the amplitude of the coupled single-particle wave functions at small separations. The use of Eq. (12) implicity assumes that, for the purposes of calculating the momentum density $F(p_q)$, the neutron-proton pair have zero separation at the instant of photoabsorption. This approximation may seem quite unreasonable because of the well-known hard-core repulsion of the NN interaction at small separations. However, the approximation is only applied to the position coordinate of the single-particle

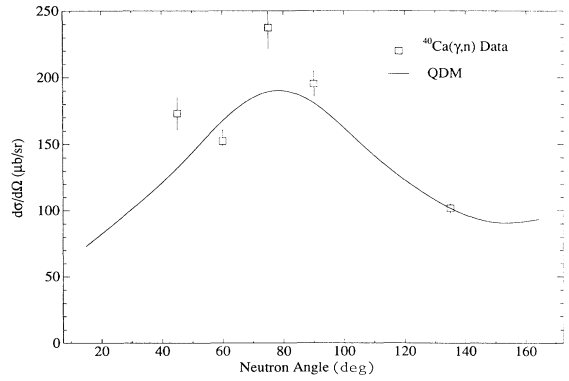

FIG. 6. ^{40}Ca(γ, n) inclusive differential cross sections.

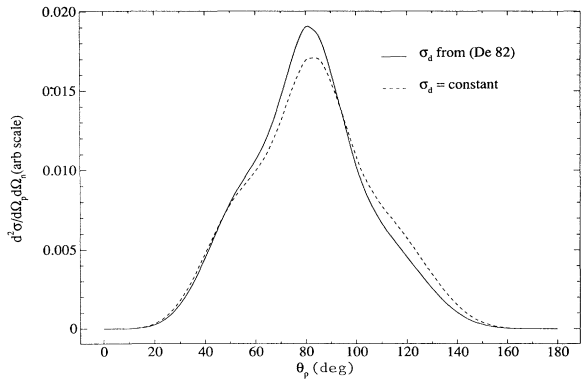

FIG. 7. QDM angular correlation function for $E_\gamma = 80$ MeV and $\theta_n = 80°$. The solid line is the standard QDM, and the dashed line is QDM with deuteron cross section set to a constant.

wave functions, and not to the separation dependence of the short-range correlation functions, so the Gottfried factorization might be regarded as an acceptable simplification, at least up to a scale factor. It is important to note that, within the Gottfried factorization, such short-range correlation functions must be contained in S_{fi}.

From the foregoing discussion, it is evident that the Gottfried-factorized cross section is insensitive to variations in S_{fi}, and is therefore insensitive to variations in the short-range correlation functions. However, in calculating the Gottfried-factorized cross section for the $^{16}O(\gamma,pn)$ reaction, Boato and Giannini [12] find extreme sensitivity to variations in the Jastrow function parameter. This flatly disagrees with the conclusions of the sensitivity study shown in Fig. 7, and requires investigation.

To resolve this discrepancy, a number of problems associated with the use of Jastrow functions are noted. First, by reference to the earlier work of Drell and Huang [39], Boata and Giannini claim that the introduction of their Jastrow correlation function does not violate the orthogonality requirement for the wave functions, although this is not consistent with the detailed study of Fink *et al.* [13]. Second, Boato and Giannini assume the NN correlation is independent of the NN separation and varies according to the displacement from the nuclear center of mass. This means that the correlation function cannot suppress the amplitude of the two-nucleon wave function at small separations, and therefore does not fulfill its intended purpose of simulating the effect of the hard-core repulsion of the NN interaction. Third, the Jastrow function is assumed to be independent of the spectroscopy of the correlated pair, although the importance of such dependence has long been established [40].

It is noted that a proper Moshinsky transformation of the correlated two-body wave functions into the (two-body) center of mass and relative coordinates is possible, and could be used with a correlation function obtained by solving the Bethe-Goldstone equation [41]. This more rigorous approach has already been persued [14] for the $^3He(e,e')$ reaction, and it was concluded that the inclusion of short-range correlations makes almost no difference for momentum transfers of less than 600 MeV/c.

It is not possible to assess the physical significance of Boato and Giannini's calculation until a more realistic correlation function is used, and adherence to the orthogonality condition is verified. If the extreme sensitivity to the Jastrow functions were confirmed, it might then be argued that the assumptions implied by the use of the Gottfried factorization are themselves dubious, and that a proper Moshinsky transformation is necessary.

For the calculation of cross sections, such as the (γ,pn) angular correlation function, where the kinematical variables are allowed to vary, but, where the spectroscopic assignments of the correlated NN pair and residual nucleus are fixed, the inclusion of short-range correlation functions should have few consequences.

The above conclusion *cannot* be extended to calculations where the spectroscopy of the final state is allowed to vary. If short-range correlations require a weight to be associated with particular spectroscopic assignments (e.g. because $S=1$ and/or $T=0$ may be more likely couplings), then the inclusion of short-range correlation functions might be necessary. The spectroscopic dependence of such short-range correlation functions could be obtained by solving the Bethe-Goldstone equation for a realistic NN potential.

V. CONCLUSIONS

The missing energy spectra for the $^{40}Ca(\gamma,n)$ reaction have been measured with tagged photons with energies ranging 31.2–57.9 and 60.5–102 MeV, for neutron emission angles of 45°, 60°, 75°, 90°, and 135°. A comparison of the results for photon energies of E_γ=60.5–102 MeV with predictions from the QDM shows good correspondence at all angles. A prescription for the calculation of a phenomenological neutron transparency correction is given, showing an explicit dependence on neutron kinetic energy and bound-state orbital. The Levinger parameter has been determined as $L=11.4\pm1.1$, and its lack of physical significance has been discussed.

Exclusive differential cross sections for the $^{40}Ca(\gamma,n)$ and $^{40}Ca(\gamma,p)$ reactions have been compared and are found to be of a similar magnitude. RPA and relativistic QDK calculation results have been compared with the data, but do not accurately predict the magnitudes of the experimental results. These calculations have been examined in detail and appear to adopt a number of questionable simplifications.

A study of the QDM angular correlation function shows that the calculated cross section is insensitive to a serious misrepresentation of the quasideuteron photoabsorption probability. This result has been generalized to question the importance of short-range correlations calculated within the Gottfried factorization.

ACKNOWLEDGMENTS

This work was supported by the Australian Research Grant Committee and the Department of Industry, Technology and Commerce. One of the authors (J.A.E.) was supported financially by the University of Melbourne. Sincere thanks are extended to Prof. R. O. Owens for providing the $^{40}Ca(\gamma,p)$ data prior to publication.

---

* Present address: The Institute für Theoretische Physik, Ruhr Universität Bochum D-4630, Germany.

† Present address: College of General Education, Tohoku University, Sendai 980, Japan.

‡ Present address: Institute for Nuclear Study, University of Tokyo, Midori-cho, Tanashi, Tokyo 188, Japan.

[1] D. J. S. Findlay and R. O. Owens, Nucl. Phys. **A279**, 385 (1977).

[2] W. Weiss and M. G. Huber, Nucl. Phys. **A162**, 330 (1971).
[3] H. Schier and B. Schoch, Nucl. Phys. **A229**, 93 (1974).
[4] S. Boffi, C. Giusti, and F. D. Pacati, Nucl. Phys. **A359**, 91 (1981).
[5] M. Gari and H. Hebach, Phys. Rep. **72**, 1 (1981).
[6] M. Cavinato, M. Maringoni, and A. M. Saruis, Nucl. Phys. **A422**, 237 (1984).
[7] J. Ryckebusch, M. Waroquier, K. Heyde, J. Moreau, and D. Ryckbosch, Nucl. Phys. **A476**, 237 (1988).
[8] H. Göringer, B. Schoch, and G. Lührs, Nucl. Phys. **A384**, 414 (1982).
[9] P. D. Harty *et al.*, Phys. Rev. C **37**, 13 (1988).
[10] M. G. Huber, Ann. Phys. **5**, 239 (1970).
[11] R. Jastrow, Phys. Rev. **98**, 1479 (1955).
[12] L. Boato and M. M. Giannini, J. Phys. G **15**, 1605 (1989).
[13] M. Fink, H. Hebach, and H. Kümmel, Nucl. Phys. **A186**, 353 (1972).
[14] J. Dubach, J. H. Koch, and T. W. Donnelly, Nucl. Phys. **A271**, 279 (1976).
[15] D. J. Gibson, Ph.D thesis, Glasgow University (1979); R. O. Owens, private communication.
[16] K. Gottfried, Nucl. Phys. **5**, 557 (1958).
[17] T. Tamae *et al.*, IEEE Trans. Nucl. Sci. **NS-30**, 3235 (1983); T. Tamae *et al.*, Nucl. Instrum. Methods **A264**, 173 (1988).
[18] T. Terasawa *et al.*, Nucl. Instrum. Methods **A248**, 4291 (1986).
[19] P. D. Harty, Ph.D thesis, The University of Melbourne (1986).
[20] J. A. Eden, Ph.D thesis, The University of Melbourne (1990).
[21] H. W. Koch and J. W. Motz, Phys. Rev. **31**, 920 (1959).
[22] R. Kurz, University of California Report UCRL 11339.
[23] D. J. Hughes and R. B. Schwartz, Brookhaven National Laboratory Report BNL 325, Suppl. No. 1, 1957.
[24] H. S. Camarda, T. W. Phillips, and R. M. White, Phys. Rev. C **34**, 810 (1986).
[25] E. Storm and H. Israel, Nucl. Data Tables. **A7**, 565 (1970).
[26] S. Fernbach, R. Serber, and T. B. Taylor, Phys. Rev. **75**, 1352 (1949).
[27] K. A. Brueckner, R. Serber, and K. M. Watson, Phys. Rev. **84**, 258 (1951).
[28] M. Sakakura, A. Arima, and T. Sebe, Phys. Lett. **61B**, 335 (1976).
[29] M. M. Giannini and G. Ricco, Rev. Nuovo. Cim. **8**, No. 4 (1985).
[30] H. Arenhövel, Z. Phys. A **302**, 25 (1981).
[31] S. Boffi, R. Cenni, C. Giusti, and F. D. Pacati, Nucl. Phys. **A420**, 38 (1984).
[32] J. P. McDermott, E. Rost, J. R. Shepard, and C. Y. Cheung, Phys. Rev. Lett. **61**, 814 (1988).
[33] A. C. Odian, P. C. Stein, A. Wattenberg, B. Feld, and R. Weinstein, Phys. Rev. **102**, 836 (1956).
[34] A. Wattenberg, A. C. Odian, P. C. Stein, H. Wilson, and R. Weinstein, Phys. Rev. **104**, 1710 (1956).
[35] M. Q. Barton and J. H. Smith, Phys. Rev. **110**, 1143 (1958).
[36] J. L. Garvey, B. H. Patrick, J. G. Rutherglen, and I. L. Smith, Nucl. Phys. **70**, 241 (1965).
[37] I. L. Smith, J. L. Garvey, J. G. Rutherglen, and G. R. Brookes, Nucl. Phys. **B1**, 483 (1967).
[38] S. N. Dancer *et al.*, Phys. Rev. Lett. **61**, 1170 (1988).
[39] S. D. Drell and K. Huang, Phys. Rev. **91**, 1527 (1953).
[40] J. G. Zabolitzky and M. Gari, H. Kümmel, Nucl. Phys. **A155**, 526 (1970).
[41] A. Kallio and B. D. Day, Nucl. Phys. **A124**, 177 (1969).